General mechanism and mitigation for strong adhesion of frozen oil sands on solid substrates

Qimeng Yang,[†] Nikoo Moradpour,[†] Jae Bem You,[*,‡] Dehui, Wang,[¶] Boran Tian,[§] Shaofeng Sun,[§] Qi Liu,[†] Xu, Deng,[¶] Dan Daniel,[‖] and Xuehua Zhang[*,†]

†*Department of Chemical and Materials Engineering, University of Alberta, Alberta T6G 1H9, Canada*

‡*Department of Chemical Engineering, Kyungpook National University, Daegu 41566, Republic of Korea*

¶*Center for Materials Surface Science, Institute of Fundamental and Frontier Sciences, University of Electronic Science and Technology of China, Chengdu 610054, P. R. China*

§*Imperial Oil, Calgary, Alberta T2C 4P3, Canada*

‖*Institute of Materials Research and Engineering (IMRE), Agency for Science, Technology and Research (A*STAR), Singapore 138634, Singapore*

E-mail: jb.you@knu.ac.kr; xuehua.zhang@ualberta.ca

Abstract

Oil sands adhered on truck bed reduce transport capacity of the truck, require manual cleaning, and create hurdles for automated surface mining. Study on the adhesion properties of oil sands to solid substrates is important to minimize the fouling of substrates during mining operation. In this work, we study the influence of hydrophobicity and mechanical properties of the substrates on the adhesion strength of frozen oil sands. By using an adhesion force apparatus with temperature control, we measure the adhesion strength of both ice and frozen oil sands on six types of substrates with

water contact angle from ∼20° to ∼130° and Young's modulus from a few MPa to 300 GPa. A clear linear correlation between the adhesion strength of pure ice and that of frozen oil sands is observed. Furthermore, the adhesion strength increases with the load on the oil sands sample, and reaches a plateau at ∼450 kPa. The maximum adhesion strength may be due to the limit of particle packing of oil sands. We also demonstrate that spray coating of anti-freezing liquids is effective for the mitigation of the adhesion of frozen oil sands. Substrates coated with various anti-freezing liquids showed undetectable oil sands adhesion strength at -20 °C with 0.06 MPa of load. The study on oil sands adhesion and potential fouling mitigation method may provide a potential solution to industries looking to reduce fouling of surfaces by frozen granular matter.

Introduction

As a complex granular matrix in nature, oil sands typically consist of 80 to 90 wt% sand (including silica, clay, and other minerals), 8 to 13 wt% of bitumen (saturates, aromatics, resins, and asphaltenes),[1,2] and 2 to 8 wt% of water.[2–5] Accumulation of oil sands to the surface of truck bed and canopy cause serious fouling problems in the oil sands industry. As shown in Figure 1, the adhered oil sands reduce transport capacity of the trucks, consume excess amount of fuels to transport the carryback after dumping, and require cleaning processes by steaming or manual scarping. The fouling issue appears to be more serious in winter than in warmer seasons. The estimated cost is several million dollars per year for one fleet working on the mining site. Therefore, it is important to understand the mechanism behind the strong adhesion of oil sands at low temperature and identify potential approaches for mitigation.

When quantifying macroscopic ice adhesion to a solid surface, the most common method is to measure the force F required to dislodge an ice block of known contact area A, i.e., $\tau = F/A$,[6,7] under shearing stress. The hydrophobicity and softness of the solid substrate

Figure 1: Example photo of oil sands fouling on truck after dumping.

were reported to decrease the ice adhesion strength (τ_{ice}) in the literature. The difference in the stiffness between ice and a soft substrate leads to stress concentration at the ice-substrate interface, which facilitates the detachment of ice from the the substrate by creating cracks at the interface.[8,9] Among the materials for soft coatings to achieve low ice adhesion, poly(dimethylsiloxane) (PDMS) − a silicone-based elastomeric polymer − has been studied the most, due to its natural hydrophobicity and tunable mechanical properties.[7,10–12] To further decrease the ice adhesion strength on PDMS substrates, modification of the surface structure is a feasible method. Combined with the surface micro/nano-structures, PDMS substrate can achieve superhydrophobicity, and the ice adhesion strength can be reduced to less than 20 kPa.[13,14] Oil infusion into PDMS substrates can reduce the ice adhesion even further (< 10 kPa).[15] However, the durability of the lubricated PDMS substrate is influenced by the depletion of the lubrication oil layer by the icing-deicing cycles.[16,17]

We recently showed that at temperatures below the freezing point of water, the adhesion of oil sands increases rapidly, and the adhesion strength of oil sands is strongly correlated to the water content.[18] However, the effects from substrate properties and from the load sustained by the oil sands on the adhesion strength on solid substrates remain unclear.

For natural oil sands, a certain amount of porosity exists within the matrix with voids not occupied by either bitumen or water.[19–21] The porosity of oil sands matrix influences the mechanical properties and behaviours of the oil sands, for example, under the shearing stress.[22] The volume of the void space depends on the water contents, which can reach 25 v% for oil sands with 4 wt% of water under 0.06 MPa of load.[18] With increasing load, the volume of the void spaces in the matrix would be lower.[21,23]

In this work, we show that the adhesion of oil sands resembles the adhesion behavior of ice on the same kind of substrates, for both hard substrates (with Young's modulus on the order of GPa) and soft substrates (Young's modulus on the order of MPa). On steel, we found a correlation between the load on the sample and the adhesion strength of frozen oil sands, attributed to the packing mode of the sand particles. The anti-freezing liquids showed high potential to reduce the adhesion strength of oil sands on steel and oil sands-fouled substrates. The strategy is also applicable at a larger scale (around 500 cm^2), which is promising for commercial application in the oil sands industry.

Materials and methods

Preparation of oil sands samples

Oil sands sample (Imperial Oil, Canada) was homogenized under ambient condition and stored in sealed plastic bags at -18 °C, as reported in our previous work.[18] The oil sands samples used in this study naturally contained 4 wt% of water, 13 wt% of bitumen and 83 wt% of solids.[18] To prevent evaporation of water, the vessel containing the homogenized oil sands were sealed with paraffin films till the samples were fully unfrozen before each measurements.

Preparation and characterization of substrates

Six types of substrates were used in this work. The substrates can be classified as hard and soft, based on their Young's moduli. The hard substrates include Silicone-epoxy-coated steel substrate (Silikopon EF, Evonik, Germany), chromium-carbide-overlay (CCO) (Imperial Oil, Canada), and steel 304 (McMaster-Carr, USA). The soft substrates are oil-resistant Buna-N nitrile rubber (McMaster-Carr, USA), poly(dimethylsiloxane) (PDMS) (Sylgard 184, Dow Corning, USA), and structured PDMS. Table 1 lists the Young's moduli of the selected substrates, which were cited from literature, except for the rubber substrate, which was provided by the vendor (Macmaster-Carr).

For hard substrates, the steel substrate was cut into square-shaped plates with the dimensions of 4 $cm \times 4$ cm. CCO was first cut into rectangular-shaped plates with the dimensions of 7 $cm \times 5$ cm, and polished by a diamond grinding wheel (D150N100b1/8, USA) mounted on a surface grinder for 30 min. To fabricate the silicone-epoxy coated steel substrate, the elastomer base, Silikopon EF, was mixed rigorously with the curing agent, (3-Aminopropyl) triethoxysilane (APTES) (>99%, Sigma, USA), by weight ratio of 4.5:1.[24] After applying about 2 g of the mixed prepolymer to a cleaned steel substrate, the fully coated substrate was put under ambient temperature for over 24 hr to cure.

For soft substrates, oil-resistant Buna-N nitrile rubber were cut into the same shape as the steel plates, with the dimensions of 4 $cm \times 4$ cm. To fabricate the PDMS substrate, a base and a curing agent (Sylgard 184, Dow Corning, USA) were mixed rigorously at a weight ratio of 10:1. About 2 g of the mixed elastomer was cast onto a clean glass slide (7 $cm \times 2$ cm) to fully cover the slide surface with a thickness of about 1 mm. After degassing for 30 min and curing at the temperature of 80°C for 2 hours, the substrate coated with PDMS were placed under ambient conditions to cool down before use. The structured PDMS substrate was fabricated in a square shape with the dimensions of 6 $cm \times 6$ cm. The structured PDMS was fabricated using standard photo- and soft lithographic methods.[25] The scanning electron microscopic (SEM) images were taken by Zeiss Sigma Field

emitting Scanning Electron Microscope. The detailed fabrication procedure and the images are provided in the Supplementary Information (Figure S1). Before use, all the substrates were rinsed with acetone (>99.5%, Fisher), ethanol (>99%, Fisher), and deionized water. The reagents (acetone and ethanol) were used as received without additional treatment. The contact angles of water on the substrates were determined by using a contact angle instrument (DSA100 system, Kruss, USA). The advancing and receding contact angles of water are shown in Table 1.

Table 1: Contact angle of water and Young's modulus of substrates

Substrate	θ_{adv} (°)	θ_{rec} (°)	Hysteresis (°)	Young's modulus
Stainless steel	92±2	21±4	71	∼200 GPa[26]
CCO	71±3	20±4	51	∼300 GPa[27]
Silikopon EF	100±3	69±4	31	∼3 GPa[24]
Rubber	109±3	58±3	51	3.2 MPa
Bare PDMS	121±3	47±4	74	1 MPa[28]
Structured PDMS	151±4	120±10	31	1 MPa[28]

To simulate the industrial environment where the substrate is often fouled by oil sands stain, we also prepared steel substrates with a layer of oil sands. To coat the steel substrate with oil sands, about 10 g of oil sands with a water content (C_w) of 10 wt% was smeared uniformly on a piece of steel plate and pressed with a load of 0.06 MPa for close contacting. C_w of the fouling layer is higher than the natural value (4 wt%) to achieve a more distinguishable result. The fabrication of oil sands with C_w higher than 4 wt% was described in our previous work.[18] After removing the excess oil sands not touching the substrate, the coated substrate was placed in a freezer at a temperature of -10 °C for 1 hr. To avoid contamination and eliminate the variation in water content of the oil sands layer, the coated substrate was wrapped in a paraffin film before being placed in the freezer. The substrate was stored in the freezer until the experiment to prevent the oil sands from thawing.

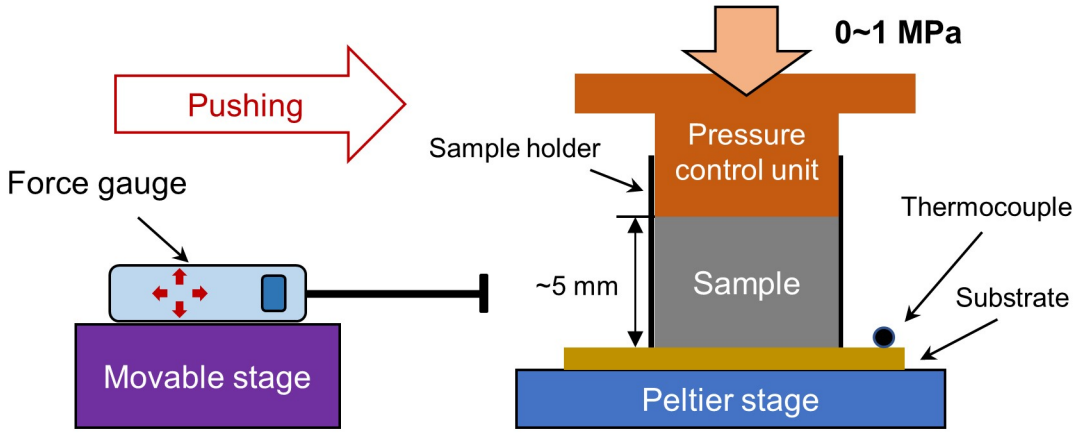

Figure 2: Schematic of adhesion strength measurement device. The sample filling in the sample holder was around 5 mm in height under a load between 0 and 1 MPa. The sample holder was cylindrical with a inner diameter of 7.2 mm, and the contact area between sample and the substrate was around 40 mm^2. The temperature range of the Peltier stage was 0 to -20 °C.

Measurements of adhesion strength

To measure the adhesion strength of frozen oil sands (τ_{os}) and ice (τ_{ice}) to a solid substrate, we built a custom device which was described in detail in our previous work[18] (Figure 2). Either water (0.2 mL) or oil sands (0.3 g) were placed in a cylindrical sample holder. The height of the sample in the holder was kept at 5 mm. For the oil sands, a homemade stage (labeled as pressure control unit in the figure) with the same base diameter of the sample holder was placed on the sample to ensure good contact with the substrate. By varying the weight loaded on the pressure control unit, we could control the pressure between the sample and the substrate from 0 to 1 MPa.

After placing the load on the sample, the Peltier stage was switched on to bring down the temperature of the substrate to -10 °C for freezing. A thermocouple was attached onto the substrate to monitor the temperature. The temperature variation of our setup was within ±1 °C, as shown in our previous work.[18]

Once the sample was frozen, the load on the pressure control unit was removed and the minimal detaching force of the sample from the substrate was measured by a digital force gauge attached to a movable stage. The maximum value measured before the sample was

pushed off from the substrate was recorded as the detaching force. The adhesion strength (τ) of the sample to the substrate was calculated by dividing the detaching force by the contact area (40 mm^2).

Larger scale tests for removal of frozen oil sands

To test the feasibility of anti-freezing liquid spray for easy removal of frozen oil sands, we conducted the adhesion measurement of oil sands (C_w = 4 wt%) on a large stainless steel plate (1.2 m × 0.6 m) sprayed with ∼100 mL of ethylene glycol (EG) solution (EG:water = 2:1). Subsequently, about 5 kg of oil sands were spread on the steel substrate under ambient condition. The possible contact area between oil sands and the coated substrate was 530,000 mm^2. An additional load from a box with a weight of around 53 kg was placed on the oil sands, creating a load of ∼0.01 MPa, as shown in Figure 3.(a). After loading, the substrate with oil sands was transferred into a walk-in freezer and was kept at -18 °C for over 2 hr. After freezing, the load was removed and the substrate was held vertically to check if the oil sands can be removed by gradually adding a lateral pushing force, as shown in Figure 3.(b). The pushing force was applied by gently placing a cardboard on the oil sands and adding a weight from the top to make the force parallel to the steel plate. The test was also performed with pristine, uncoated stainless steel substrate as control.

Results and discussion

Effects of load on oil sands adhesion strength

Figure 4.(a) showed the representative plots of force/stress versus time under the load of 0.03 MPa (shown in color red) and 0.6 MPa (shown in color green). The slopes of the curves for all samples were similar to each other, indicating that the pushing velocity from the movable stage was reliable over repeated experiments. The colored boxes in Figure 4.(a) represent the range of variation in the adhesion force (F_{os})/strength (τ_{os}) for the samples. As

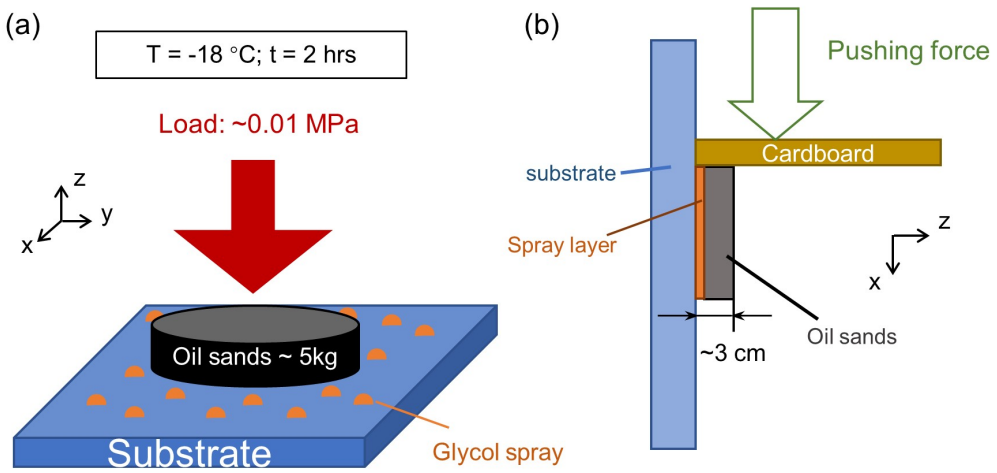

Figure 3: Schematic of large scale test procedure with the glycol spray. (a) - Process of oil sands sample freezing on the substrate sprayed with anti-freezing liquids under a load of ~0.01 MPa; (b) - Process of oil sands removal after frozen by adding weight on the cardboard.

shown, the boxes were narrow enough showing that both F_{os} and τ_{os} for all tested samples were measured with acceptable variation. After oil sands were detached from the substrate, no residual sample was observed on the substrate, justifying the rationality of normalizing by the apparent contact area between oil sands and the substrate.

In Figure 4.(b), we showed how τ_{os} varied with load applied on the oil sands samples for two different freezing times. With 15 min of freezing time, τ_{os} for oil sands rapidly increased from 0 to 450 kPa with the load on the sample from 0 to 0.1 MPa. Above the applied load of 0.45 MPa and up until 0.6 MPa, τ_{os} remained nearly plateaued at 550 kPa. τ_{os} increased with the load and eventually reached a plateau. Adhesion strength was also measured for 30 min of freezing time (shown as orange points in Figure 4.(b)). Under the same load, no apparent difference was observed between τ_{os} obtained at 15 min and at 30 min of freezing time. Therefore, it is reasonable to assume that the equilibrium freezing time is $\leq$ 15 min in our systems.

The increase in τ_{os} with the load from 0.03 to 0.1 MPa could be attributed to displacement of voids and some initial easy rearrangement of composition in oil sands. The previous work showed that after compression under 0.06 MPa of load, oil sands consisted of 55 v% of

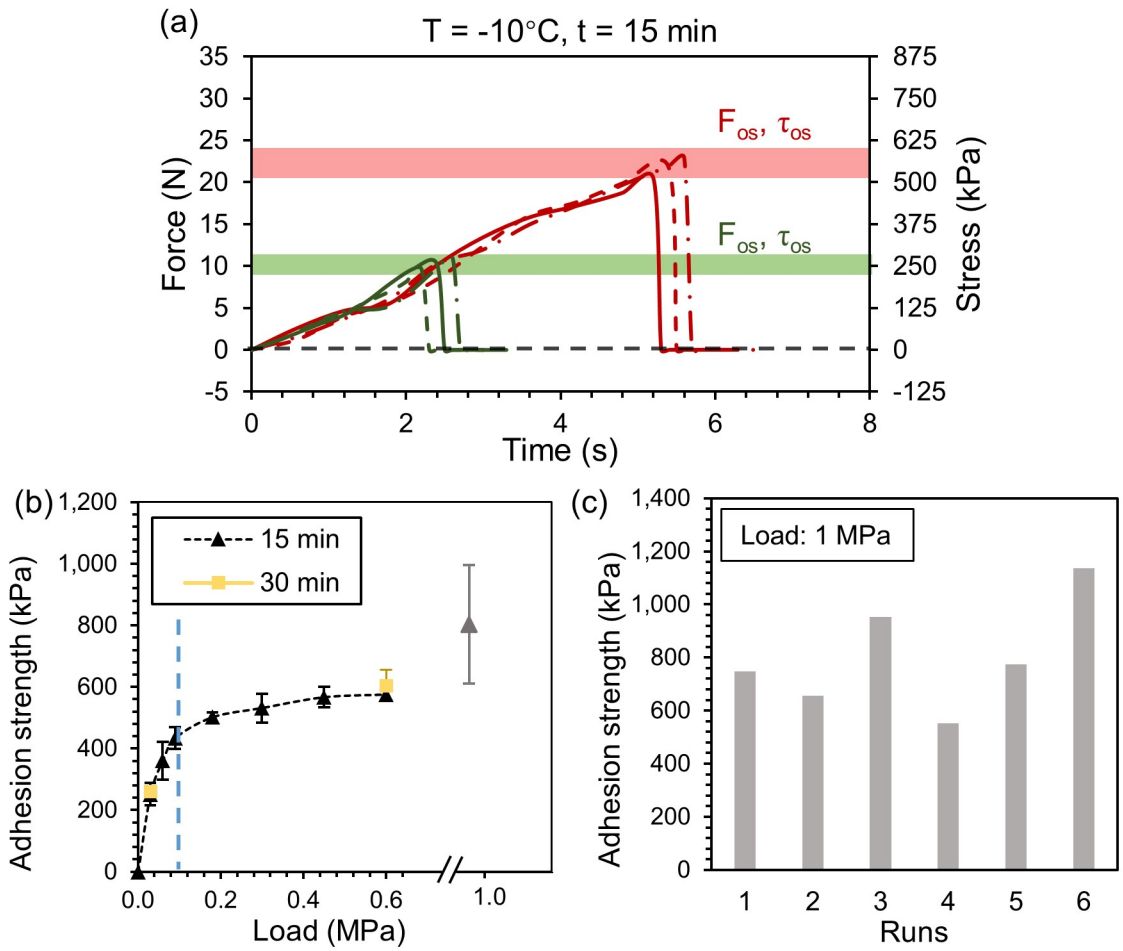

Figure 4: Effect of load on the τ_{os}. (a) - Representative force/stress curves for τ_{os} at -10 °C for 15 min of freezing. The black dashed line denotes 0 N or 0 kPa of adhesion. The lines with red/green color are for oil sands under 0.03/0.6 MPa of load. The colored stripe with corresponding color denotes the minimum detachment force (F_{ad})/adhesion strength (τ) for frozen oil sands at 0.03 (green) and 0.6 (red) MPa of load. The width of the stripe denotes the variation of 3 repeated tests; (b) - Effect of load from 0 to 1 MPa on τ_{os} with a freezing time of 15 min and 30 min. The dotted line is at 0.1 MPa. Error bars are standard deviation of at least 3 repeated measurements; (c) - τ_{os} under an extremely high load of 1 MPa with 15 min of freezing time for 6 runs.

solids, 20 v% of liquids and 25 v% of air.[18] Under the load, the contact area initially occupied by voids (air) in loose oil sands could be replaced by liquids or solid particles. Moreover, water could transfer from the sample above to the substrate through stronger capillary effects in small gaps under the compression.[23] Water accumulated at the substrate could form more bridges and larger contact area with the substrates, leading to the sharp increase in τ_{os}. As the load reached around 400 kPa and above, τ_{os} only increased slowly because of

the lower mobility and deformability of the densely packed materials in oil sands. The effect of the load on the adhesion strength of oil sands supports our argument that water contact area dominates τ_{os} for oil sands adhesion to the steel substrate.

However, at an even higher load of 1 MPa, the average value of τ_{os} increased significantly to ~800 kPa. We assume that peeling off of the bitumen layer from the sands surface under a high load may lead to an increase in the contact between water and the substrate surface. It was shown in the literature that the ultrasound and CO_2 pressure could enhance the bitumen liberation during the extraction process.[29,30] The liberated bitumen may spatially rearrange, and the composition in the oil sands matrix may pack more densely, and thus, lead to higher adhesion strength. The large variation in τ_{os} under 1 MPa of load (Figure 4.(b)) may be attributed to random redistribution of the granular structure in each test.

Effects of surface properties on adhesion strength

τ_{os} and τ_{ice} on six substrates (shown in Table 1) were compared. Among them, hard CCO is the most hydrophilic substrate (lowest advancing contact angle of ~70°), and soft structured PDMS is the most hydrophobic with the highest advancing contact angle of 151° and receding angle of over 120°. The influence of contact angle on ice adhesion strength on hard and soft substrates is shown in Figure 5.(a). Structured PDMS yielded the lowest ice adhesion strength (τ_{ice}= 39 kPa). On the other hand, τ_{ice} on CCO was dramatically higher, 817 kPa. τ_{ice} on steel is too high to be measured within the detectable range of the force gauge in our apparatus. From the literature, τ_{ice} on steel is ~1,250 kPa.[31,32]

Theoretical description of the relationship between ice adhesion strength and static water contact angle has been reported in the literature.[33] Thermodynamic work of adhesion of water on the substrate is expressed as below.

$$\tau = C_0(1 + cos\ \theta_{rec}) \quad (1)$$

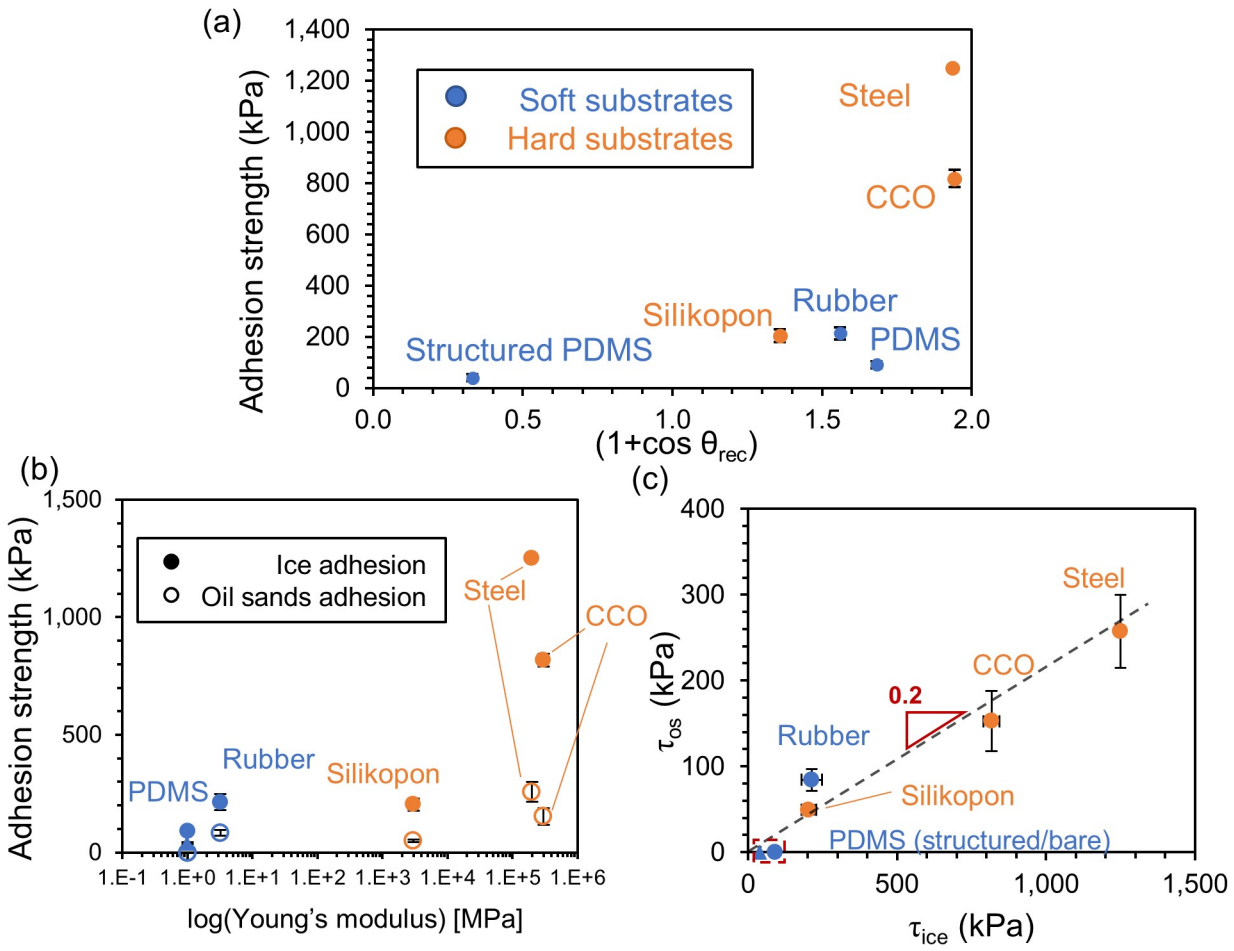

Figure 5: Effect of substrate surface properties on ice/oil sands adhesion strength on hard (Silicopon, CCO, and steel) and soft substrates (rubber, PDMS, and structured PDMS). (a) - τ_{ice} to work of detachment of water $(1 + \cos\,\theta_{rec})$ on hard (orange) and soft substrates (blue); (b) - τ_{os} and ice on both soft and hard substrates with the Young's modulus of the substrates in MPa. The oil sands were under 0.03 MPa of load before frozen; (c) - Linear relationship between τ_{os} and τ_{ice} on 6 substrates. τ_{os} on PDMS substrates (structured and bare) is below the minimum detectable range of our setup ($\sim$2 kPa), labeled as 0 kPa on the plots. Error bars are standard deviation of at least 3 repeated measurements.

where τ is ice adhesion strength in kPa, C_0 is a constant also in kPa related to the surface tension of water, and θ_{rec} is the receding contact angle of water on the substrate. According to Eq.1, a linear correlation between the adhesion strength and cos θ_{rec} is expected. However, as shown in Figure 5 (a), the adhesion strength is strongly influenced by the properties of the substrates such as hardness and surface roughness.

For hard substrates, namely, Silikopon, steel and CCO, the ice adhesion increases with

surface roughness which can be deduced from the contact angle hysteresis values. It has been reported that the surface roughness of the substrates can increase the ice adhesion[34–36] by increasing the contact area between ice and substrate. As shown in Table 1 and Figure 5 (a), the high contact angle hysteresis ($\theta_{adv} - \theta_{rec}$) of CCO and steel may be related with the high surface roughness of the two substrates, which may explain the reason for the high τ_{ice} as compared to the Silikopon EF substrate.

On the other hand, for soft substrates, deformability also influences the adhesion strength. The Young's modulus of ice is known to be on the order of 8 to 10 GPa,[37,38] which is at least 1,000 times higher than that of PDMS ($\sim$ 1 MPa) and rubber substrates ($\sim$ 3.2 MPa). Mismatch between the moduli of ice and soft substrates can cause stress concentration at the interface which can facilitate ice detachment under shear stress and ice sliding on the soft substrate.[11,25] As shown in Figure 5 (a), the adhesion strength for the rubber substrate is higher than that of bare PDMS despite the fact that the rubber has higher θ_{rec}. Therefore, in this case, an interplay between the surface energy, surface roughness and substrate modulus determines the adhesion. In the case for structured PDMS sample, the ice-solid contact area is much lower compared to that of the rubber and flat PDMS, which additionally decreases the ice adhesion.

Importantly, on both hard and soft substrates, we demonstrated a clear correlation between τ_{os} and τ_{ice}. The oil sands were pressurized with 0.03 MPa of load during freezing. As shown in Figure 5.(b), both τ_{ice} and τ_{os} increased with the Young's modulus of the substrate. Interestingly, τ_{os} on bare and structured PDMS surface were even below the minimum detectable range of our setup (< 2 kPa), in agreement with the low τ_{ice} on PDMS substrate (< 100 kPa). Results in Figure 5.(b) suggest that for structured PDMS, the contents in the oil sand matrix (i.e. sand particles and bitumen) may not penetrate into the microstructure. Otherwise, the effect of mechanical interlock would have increased τ_{os} on structured PDMS. Thus, the low τ_{os} on structured PDMS substrate is an indicator that the oil sands stayed on top of the microstructures of the PDMS substrate with air filling the gaps, much like in

'Cassie-Baxter' state.

Figure 5.(c) shows that the adhesion strength of oil sands τ_{os} increases with the ice adhesion τ_{ice} on both soft and hard substrates. In our recent work, we demonstrated the critical role of ice formation in the adhesion strength of a wet granular matter (oil sands) at low temperature.[18] Freezing of water bridges formed between water in oil sands and the substrate led to strong adhesion of frozen oil sands. The close correlation between τ_{os} and τ_{ice} in Figure 5.(c) further confirms that the ice formation on the solid surface is the primary reason for the adhesion strength of frozen oil sands.

The slope of the linear fitting in Figure 5.(c) is 0.2, suggesting that the surface coverage of ice on all six substrates is around 20%. Considering the weight percentage of each component in oil sands (4 wt% of water, 13 wt% of bitumen and 83 wt% of solids) and the density of each component (1 g/cm^3 for water and bitumen and 2.6 g/cm^3 for sands), the maximal volume fraction of water is ∼10 v% in oil sands assuming no void space is present. The maximal surface coverage of water on the substrates is estimated to be $(10\ \text{v}\%)^{2/3} \approx 0.22$, which is in good agreement with the slope of the linear fitting.

Mitigation of adhesion by anti-freezing liquid

Spraying a layer of anti-freezing liquid such as ethylene glycol is an effective approach to reduce the adhesion strength of oil sands.[18] Here, to explore the applicability of anti-freezing liquids, we tested aqueous solutions of ethylene glycol and propylene glycol, which were reported to reduce the freezing point of water down to -40 °C in principle.[39,40] The solutions were spray coated on target substrates prior to testing them for the adhesion of frozen oil sands. The stability of the sprayed droplets were evaluated after evaporating under ambient condition and after spinning. The detailed procedure of the stability tests was provided in Supplementary Information (Figure S2) and the EG droplets remained stable after 3 hr of evaporation and could hold a stress equivalent to 60 kPa. Figure 6 shows the adhesion strength of the frozen oil sands sample on the substrates coated/uncoated by one type of

anti-freezing solution – EG:water = 2:1.

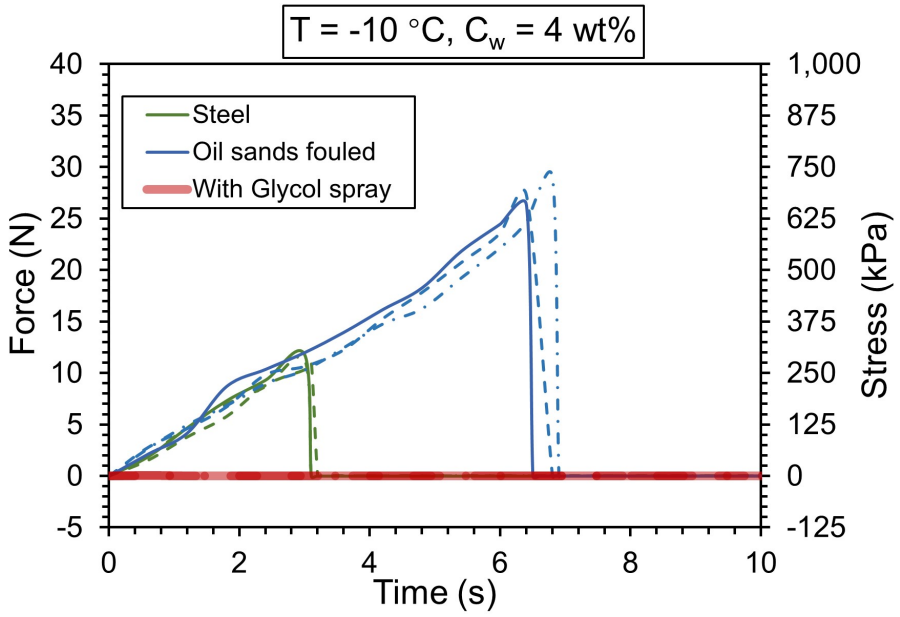

Figure 6: Representative force curves for oil sands adhesion strength on steel/oil sands fouled layer with/without glycol spray (EG:water = 2:1). Adhesion tests were performed with frozen oil sands with natural water concentration of 4 $wt\%$ under 60 kPa of load. The freezing temperature and time were -10 °C and over 15 min. The value of force and stress is all 0 for the case with glycol spray with 3 repeated tests (shown as 3 types of red lines in the figure).

In Figure 6, apart from pristine steel substrates ($\tau_{os} \approx 250\ kPa$), we also measured τ_{os} on the pre-fouled oil sands layer. The adhesion strength of oil sands with C_w of 4 wt% was over 700 kPa, which was around three times as the adhesion strength of oil sands to the bare steel substrate under the same conditions, demonstrating a stronger adhesion strength of oil sands to the fouled substrate. However, with the outstanding performance of spraying a layer of glycol solution, τ_{os} on both pristine and fouled substrates reduced to an almost undetectable level at -10°C. Table 2 lists the condition and the adhesion strength of the frozen samples on the substrates coated by the anti-freezing solutions with different compositions. As shown by the table, the τ_{os} on all of the spray coated substrates were lower than the detection limit of the experimental apparatus, which was around 2 kPa.

From the data listed in Table 2, we could see that by spraying anti-freezing liquids with multiple compositions, τ_{os} decreased to almost undetectable not only on pristine steel

Table 2: Conditions and results of τ_{os} measurement with anti-freezing liquid spray.

Substrate	Anti-freezing liquid (v/v)	τ_{os}
Steel	Without spray	~250 kPa
Steel	EG:water = 3:1	<2 kPa
Steel	EG:water = 2:1	<2 kPa
Steel	PG:water = 3:1	<2 kPa
Steel	PG:water = 2:1	<2 kPa
Oil sands-fouled	Without spray	~700 kPa
Oil sands-fouled	EG:water = 2:1	<2 kPa
Oil sands-fouled	PG:water = 2:1	<2 kPa

substrate, but also on the oil sands-fouled substrates, which naturally has higher τ_{os}. In the oil industry, the surfaces are commonly pre-fouled by oil sands. In this case, the possibility for the spray to reduce the adhesion strength between oil sands and the pre-fouling layer endows it a broader application for anti-fouling purpose in the industry.

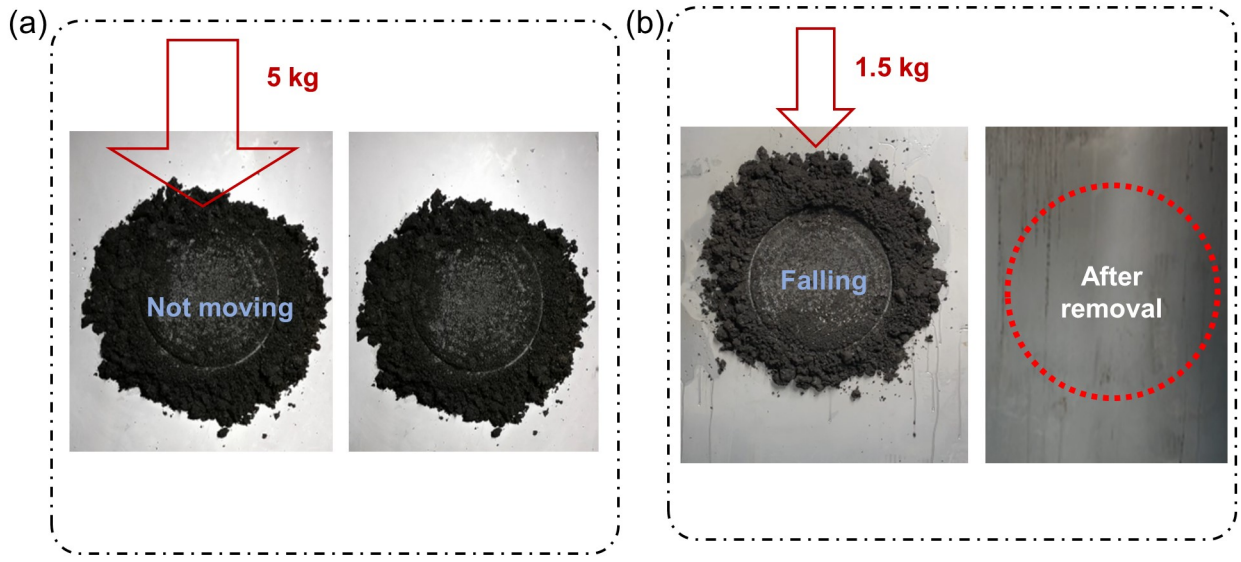

Figure 7: Effects of EG spray (EG:water = 2:1) on reducing oil sands adhesion at large scale. Snapshots were taken from the video recording of the removing process in the walk-in freezer after the oil sands were frozen at -18 °C for 2 hr. Videos are provided in Supplementary Information (video S1 & S2). (a) - Without anti-freezing liquid spray, oil sands could not be removed with 5 kg of load; (b) - with anti-freezing liquid spray, oil sands could be easily removed with 1.5 kg of load. No stain was observed after swiping with acetone in the freezer.

The anti-fouling performance of anti-freezing liquid was also tested at large scale as shown in Figure 7. Detailed testing procedure is discussed in the Experimental section.

For substrates without anti-freezing coating, oil sands could not be removed with $\sim$5 kg of load nor by swiping with acetone at -18 °C. In contrast, for the substrates with EG coating (Figure 7.(b)), the frozen oil sands can be easily removed with $\sim$1.5 kg of load on the oil sands sample. Only slight stain of bitumen was left after oil sand fell of the substrate. The bitumen stain can be cleaned with acetone swipe in the freezer, and the steel substrate after cleaning was almost as clean as the condition before the test. The result indicates that by spray coating anti-freezing liquid onto steel substrate, it is possible to remove the oil sands carryback, and thus save the time and energy consumption from the traditional scrapping method.

The cost of the spray (EG:water = 2:1) is estimated by multiplying the price per volume of the spray with the estimated total volume of spray on the truck for each year. From the photo shown in Figure S2, it is reasonable to assume the spray on the steel substrate is a layer of uniform coating with a thickness of $\sim$10 μm. The price of ethylene glycol on the market is $\sim$1,000 CAD/m^3. Considering that the total area of the truck bed and canopy is around 75 m^2 for 797F mining truck (one type of truck working on the oil sands mining spot), the cost for each truck for each run will be only 0.5 CAD. From the field data, each truck takes around 6,000 run to transport the oil sands from the mining spot in each winter, and there are less than 100 trucks working on the field at the same time. Assuming that the spray is required after each run of transportation, the total cost of the spray for one fleet each year is estimated to be $\sim$0.3 million CAD.

Conclusion

In this work, we showed that the adhesion of frozen oil sand is affected by the substrate type as well as the load applied to the sand. Ice adhesion strength on all six substrates in our experiments was found to correlate linearly with the adhesion strength of frozen oil sands. Higher load was found to increase the adhesion strength, possibly due to increased

contact area with water in compact matrix of oil sands. Up to a plateau load (i.e., 450 kPa), additional load could not increase the adhesion strength any further. The maximum adhesion strength may be due to the limit of particle packing of oil sands. Anti-freezing liquid was proved to effectively reduce the adhesion strength for oil sands to less than 2 kPa under the freezing point of water. Applying anti-freezing liquid was effective in reducing adhesion on all tested substrates including pristine steel and oil sands-fouled substrates. The method of spray-coating of anti-freezing liquid may provide a solution for eliminating carryover in transport of oil sands in cold regions, as the method is time effective and easy to implement with potential applications for autonomous mining.

Acknowledgement

The authors acknowledge the funding support from the Institute for Oil Sands Innovation (IOSI) (Project number IOSI 2019-11) and from the Natural Science and Engineering Research Council of Canada (NSERC). Part of the research is supported by Canada Research Chair program. The authors are grateful for technical support from the IOSI lab, particularly from Xiaoli Tan, Lisa Brandt and Brittany MacKinnon for their help in experiment training and supervision. The authors are also grateful for Gilmar F. Arends's help in the large scale tests,for Qiuyun Lu in taking SEM images, and for Binglin Zeng in contact angle measurements.

References

(1) He, L.; Li, X.; Wu, G.; Lin, F.; Sui, H. Distribution of saturates, aromatics, resins, and asphaltenes fractions in the bituminous layer of athabasca oil sands. *Energy & fuels* **2013**, *27*, 4677–4683.

(2) Nie, F.; He, D.; Guan, J.; Li, X.; Hong, Y.; Wang, L.; Zheng, H.; Zhang, Q. Oil sand

pyrolysis: Evolution of volatiles and contributions from mineral, bitumen, maltene, and SARA fractions. *Fuel* **2018**, *224*, 726–739.

(3) Hepler, L. G.; Hsi, C. AOSTRA technical handbook on oil sands, bitumens and heavy oils. **1989**,

(4) Hooshiar, A.; Uhlik, P.; Liu, Q.; Etsell, T. H.; Ivey, D. G. Clay minerals in nonaqueous extraction of bitumen from Alberta oil sands: Part 1. Nonaqueous extraction procedure. *Fuel Process. Technol.* **2012**, *94*, 80–85.

(5) Nikakhtari, H.; Wolf, S.; Choi, P.; Liu, Q.; Gray, M. R. Migration of fine solids into product bitumen from solvent extraction of Alberta oilsands. *Energy & fuels* **2014**, *28*, 2925–2932.

(6) Meuler, A. J.; Smith, J. D.; Varanasi, K. K.; Mabry, J. M.; McKinley, G. H.; Cohen, R. E. Relationships between water wettability and ice adhesion. *ACS applied materials & interfaces* **2010**, *2*, 3100–3110.

(7) Beemer, D. L.; Wang, W.; Kota, A. K. Durable gels with ultra-low adhesion to ice. *J. Mater. Chem. A* **2016**, *4*, 18253–18258.

(8) He, Z.; Xiao, S.; Gao, H.; He, J.; Zhang, Z. Multiscale crack initiator promoted super-low ice adhesion surfaces. *Soft Matter* **2017**, *13*, 6562–6568.

(9) He, Z.; Zhuo, Y.; He, J.; Zhang, Z. Design and preparation of sandwich-like polydimethylsiloxane (PDMS) sponges with super-low ice adhesion. *Soft Matter* **2018**, *14*, 4846–4851.

(10) Yeong, Y. H.; Wang, C.; Wynne, K. J.; Gupta, M. C. Oil-infused superhydrophobic silicone material for low ice adhesion with long-term infusion stability. *ACS Appl. Mater. Interfaces* **2016**, *8*, 32050–32059.

(11) Wang, C.; Fuller, T.; Zhang, W.; Wynne, K. J. Thickness dependence of ice removal stress for a polydimethylsiloxane nanocomposite: Sylgard 184. *Langmuir* **2014**, *30*, 12819–12826.

(12) Khanafer, K.; Duprey, A.; Schlicht, M.; Berguer, R. Effects of strain rate, mixing ratio, and stress-strain definition on the mechanical behavior of the polydimethylsiloxane (PDMS) material as related to its biological applications. *Biomed. Microdevices* **2021**, 503–508.

(13) Urata, C.; Hönes, R.; Sato, T.; Kakiuchida, H.; Matsuo, Y.; Hozumi, A. Textured organogel films showing unusual thermoresponsive dewetting, icephobic, and optical properties. *Advanced Materials Interfaces* **2019**, *6*, 1801358.

(14) Sun, Y.; Wang, Y.; Sui, X.; Liang, W.; He, L.; Wang, F.; Yang, B. Biomimetic multiwalled marbon nanotube/polydimethylsiloxane nanocomposites with temperature-controlled, hydrophobic, and icephobic properties. *ACS Applied Nano Materials* **2021**,

(15) Liu, Q.; Yang, Y.; Huang, M.; Zhou, Y.; Liu, Y.; Liang, X. Durability of a lubricant-infused electrospray silicon rubber surface as an anti-icing coating. *Applied Surface Science* **2015**, *346*, 68–76.

(16) Golovin, K.; Kobaku, S. P.; Lee, D. H.; DiLoreto, E. T.; Mabry, J. M.; Tuteja, A. Designing durable icephobic surfaces. *Science advances* **2016**, *2*, e1501496.

(17) Zhuo, Y.; Xiao, S.; Amirfazli, A.; He, J.; Zhang, Z. Polysiloxane as icephobic materials–the past, present and the future. *Chemical Engineering Journal* **2020**, 127088.

(18) Yang, Q.; You, J. B.; Tian, B.; Sun, S.; Daniel, D.; Liu, Q.; Zhang, X. Water-mediated adhesion of oil sands on solid surfaces at low temperature. *Fuel* **2021**,

(19) Nutting, P. G. Physical analysis of oil sands. *AAPG Bulletin* **1930**, *14*, 1337–1349.

(20) Doan, D. H.; Delage, P.; Nauroy, J. F.; Tang, A. M.; Youssef, S. Microstructural characterization of a Canadian oil sand. *Canadian Geotechnical Journal* **2012**, *49*, 1212–1220.

(21) Mossop, G. D. Geology of the Athabasca oil sands. *Science* **1980**, *207*, 145–152.

(22) Dusseault, M. B.; Morgenstern, N. R. Shear strength of Athabasca oil sands. *Canadian Geotechnical Journal* **1978**, *15*, 216–238.

(23) Bacher, C.; Olsen, P.; Bertelsen, P.; Sonnergaard, J. Compressibility and compactibility of granules produced by wet and dry granulation. *International journal of pharmaceutics* **2008**, *358*, 69–74.

(24) Wu, X.; Zhao, X.; Ho, J. W. C.; Chen, Z. Design and durability study of environmental-friendly room-temperature processable icephobic coatings. *Chemical Engineering Journal* **2019**, *355*, 901–909.

(25) Wang, D.; Sun, Q.; Hokkanen, M. J.; Zhang, C.; Lin, F.-Y.; Liu, Q.; Zhu, S.-P.; Zhou, T.; Chang, Q.; He, B., et al. Design of robust superhydrophobic surfaces. *Nature* **2020**, *582*, 55–59.

(26) Ledbetter, H.; Frederick, N.; Austin, M. Elastic-constant variability in stainless-steel 304. *Journal of Applied Physics* **1980**, *51*, 305–309.

(27) Zikin, A.; Hussainova, I.; Katsich, C.; Badisch, E.; Tomastik, C. Advanced chromium carbide-based hardfacings. *Surface and Coatings Technology* **2012**, *206*, 4270–4278.

(28) Bouteau, M.; Cantin, S.; Fichet, O.; Perrot, F.; Teyssié, D. Contribution toward comprehension of contact angle values on single polydimethylsiloxane and poly (ethylene oxide) polymer networks. *Langmuir* **2010**, *26*, 17427–17434.

(29) Fu, L.; Zhang, G.; Ge, J.; Liao, K.; He, Y.; Wang, X.; Li, H. Study on dual-frequency ultrasounds assisted surfactant extraction of oil sands. *Fuel Processing Technology* **2017**, *167*, 146–152.

(30) Zhao, X. Novel green processing of oil sands: from extraction of bitumen to treatment of byproducts. Ph.D. thesis, The University of Utah, 2018.

(31) Ozbay, S.; Erbil, H. Y. Ice accretion by spraying supercooled droplets is not dependent on wettability and surface free energy of substrates. *Colloids and Surfaces A: Physicochemical and Engineering Aspects* **2016**, *504*, 210–218.

(32) Fillion, R. M.; Riahi, A.; Edrisy, A. Design factors for reducing ice adhesion. *Journal of adhesion science and technology* **2017**, *31*, 2271–2284.

(33) Makkonen, L. Ice adhesion—theory, measurements and countermeasures. *Journal of Adhesion Science and Technology* **2012**, *26*, 413–445.

(34) Fu, Q.; Wu, X.; Kumar, D.; Ho, J. W.; Kanhere, P. D.; Srikanth, N.; Liu, E.; Wilson, P.; Chen, Z. Development of sol–gel icephobic coatings: effect of surface roughness and surface energy. *ACS applied materials & interfaces* **2014**, *6*, 20685–20692.

(35) Hassan, M.; Lee, H.; Lim, S. The variation of ice adhesion strength with substrate surface roughness. *Measurement Science and Technology* **2010**, *21*, 075701.

(36) Memon, H.; Liu, J.; De Focatiis, D. S.; Choi, K.-s.; Hou, X. Intrinsic dependence of ice adhesion strength on surface roughness. *Surface and Coatings Technology* **2020**, *385*, 125382.

(37) Schulson, E. M. The structure and mechanical behavior of ice. *Jom* **1999**, *51*, 21–27.

(38) Meng, W.; Guo, Y. Experimental study on mechanical properties of ice. Proceedings of the AASRI International Conference on Industrial Electronics and Applications (IEA2015), London UK. 2015; pp 192–196.

(39) Hollis, J. M.; Lovas, F. J.; Jewell, P. R.; Coudert, L. Interstellar antifreeze: ethylene glycol. *The Astrophysical Journal Letters* **2002**, *571*, L59.

(40) Bischoff, K. Propylene glycol. *Small animal toxicology. St. Louis: Elsevier Saunders* **2006**, 996–1001.